**AALBORG UNIVERSITY**

# Impedance Measurement of Traction Network and Electric Train for Stability Analysis in High-Speed Railways

Pan, Pengyu; Hu, Haitao; Yang, Xiaowei; Blaabjerg, Frede; Wang, Xiongfei; He, Zhengyou

# Impedance Measurement of Traction Network and Electric Train for Stability Analysis in High-Speed Railways

Pengyu Pan, *Student Member, IEEE*, Haitao Hu, *Member, IEEE*, Xiaowei Yang, *Student Member, IEEE*, Frede Blaabjerg, *Fellow, IEEE*, Xiongfei Wang, *Senior Member, IEEE* and Zhengyou He, *Senior Member, IEEE*

*Abstract*—**Instability and oscillation issues have frequently occurred in high-speed railways due to the mismatch of impedances versus frequency between the 4-quadrant converter (4QC)-based high-speed train and the traction network (hereinafter train-network). However, solely utilizing the mathematical deduction to quantify the impedances appears to be difficult owing to unknown detailed parameters of both traction network and electric train. This paper proposes a method to measure the equivalent impedances of traction network and the 4QC of electric train in the stationary frame for stability analysis. A disturbance circuit consisted of anti-parallel insulated gate bipolar transistor (IGBT) modules and an excitation load is adopted by means of the pulse width modulation (PWM) signal to drive the IGBTs. Consequently, a desired broad spectral excitation is then generated to measure the output impedance of the traction network. When injecting the harmonics twice which are linearly independent at the same frequency, the input impedance of 4QC of the electric train can be calculated at the corresponding frequency considering the frequency-coupled effect. The proposed method shows a good measurement accuracy. Additionally, the stability and oscillation issues of the train-network system can be then identified using measured impedances. Both simulation and experimental results confirm the effectiveness of the proposed measurement methods.**

*Index Terms*—**Impedance measurement, low-frequency oscillation, high-speed railway, 4-quadrant converter, electric train.**

## I. INTRODUCTION

POWER electronic converters with a constant power feature may bring a negative incremental impedance to the electrical power system [1]-[7]. With increasing adoption of these constant power loads, oscillations and stability issues have been frequently aroused in industrial power systems that may potentially lead to a system collapse in serious operations [4], [5]. As a special power system, traction power system may encounter the same stability issues caused by the interaction be-

tween the electric train and traction network [6], [7]. Traction network impedance determines the strength of the network that an enough strong network can endure the negative impedance caused by the constant power loads, and a weak network may easily arise small-signal stability issues [8], [9].

Previous publications have shown that these instability issues can be avoided in some industrial power systems by improving the power electronic control for obtaining the appropriate impedance characteristics [10], [11]. These methods can provide a reference for designing the control of power electronic devices to guarantee a stable system [12], [13]. As a result, it is especially important for measuring the corresponding impedances in industrial applications.

In terms of the impedance measurement, the existing methods can be classified in two categories: passive method and active method. The former one can estimate the impedance based on the mathematical analysis and numerical processing without any disturbance injection [14]-[17]. An effective method based on recursive least-squares algorithm has been proposed in [14] to estimate the grid impedance. In order to improve the response speed of the measurement method, [15] introduced a forgetting factor into the original recursive least-squares estimation algorithm. Apart from that, the estimation model of grid impedance has been established to gradually estimate the real impedance values by adjusting the estimated values [16]. Furthermore, some inherent harmonics have occurred in the power system for the switching feature of grid-connected power converters, and they are used to access the power grid impedance [17]. As a result, the passive method has free impact on the original system. However, the accuracy of extracted impedance is usually unsatisfactory, and the speed of the impedance measurement process is slow due to its complex mathematical process.

The active method relies on the harmonic injection by means of additional power electronic devices to detect the impedance [18]-[22]. In this context, a sine waveform sweep-based technique proposed in [18] produces the most promising signal-to-noise ratio (SNR) to measure the most accurate impedance. Nevertheless, sine waveform sweeps spend much time on measuring the impedance owing to its repeated injections. In order to measure the impedance over a broad frequency range with only once injection, broad spectral excitations such as random pulse width modulation (RPWM) signals have been adopted in [19]. However, it is not easy to guarantee the accuracy of the measured impedance as the excitation energy distribution in the frequency domain is irregular and uncontrolla-

ble. Moreover, a large injected energy is required to ensure the accuracy of the impedance measurement process, yet the procedure may face a risk of disturbing the normal operation of the original system. Hence, a maximum-length binary sequence (MLBS) signal, was applied to increase the SNR and reduce the injection level, has a good performance in detecting the impedance of the strong grid, and shows a good applicability for sensitive systems [20], [21]. In addition, the discrete-interval binary sequence (DIBS) has been used to specify the range of the energy spectrum in [22], and improve the energy of the specified frequencies as much as possible without increasing the injection current amplitude.

The dynamic characteristic of the traction network in the high-speed railways varies timely, meanwhile the large-power/capacity 4QC-based electric train shows a non-linear feature. As a result, the passive method using mathematical analysis and numerical processing to estimate the real-time accurate impedance seems to be complicate and difficult. On the other hand, the more precise train-network impedances can be obtained by using the active method, which is more applicable for the small signal stability analysis of train-network system.

Therefore, this paper proposes the active method-based impedance measurement for traction network and electric train and associated stability investigation method in the high-speed railway. The main contributions are:

1) The traction network impedance at desired frequencies can be synchronously detected by imposing disturbance for only once through the proposed broad spectral excitation method, which greatly reduces the required time.

2) The impedance of the 4QC of electric train can be obtained considering the frequency coupling effect, which makes the measured 4QC impedance more accurate.

3) Before the electric train is put into operation, the measured train-network impedances can be used to forecast the stability of this system for ensuring a safe and stable operation condition.

The rest of the paper is organized as follows: an impedance measurement strategy for the traction network is introduced in Section II. Section III presents a measurement method of the 4QC of electric train considering the frequency coupling effect. Thus, the stability analysis based on the measured train-network impedances is then discussed in detail in Section IV. Section V shows the experimental validation, including the measured impedances of the train-network system as well as stability condition identification. Finally, conclusions are given in Section VI.

## II. IMPEDANCE MEASUREMENT OF TRACTION NETWORK

### A. Basic Measurement Method

The autotransformer (AT)-fed traction network is widely applied in the high-speed railways around the world, as illustrated in Fig. 1. The transformer in traction substation transforms the three-phase 110 kV/220 kV power source to two single-phase 2×27.5-kV supply phases. Electric trains obtain the energy from the catenary network. The AT substation (ATS) is located at approximately every 10 km-15 km along the railroad and the sectioning post (SP) is located between two traction substations. In the ATS and SP, an autotransformer with an

earth-connected central tap feeds two terminals: catenary and positive feeder line. In addition, the up-track and down-track catenary network are connected in parallel at ATS and SP [23], [24]. Usually the traction network only contains some special harmonic frequencies which are closed to the switching frequency of the power electronics converter as the electric railway system operates without injecting disturbance. Thus, the impedances can be measured only at these corresponding frequencies. In order to measure the impedances at the designed frequencies, an imposing disturbance is added to the system (see Fig. 1) to produce more desired harmonic components. According to the response voltage and current after imposing a disturbance, the traction network impedance in a broad frequency spectrum can be detected. Correspondingly, Fig. 2 shows the equivalent measurement model of Fig. 1, where the traction network is equivalent to an ideal voltage source $\mathbf{U}_g$ in series with the impedance $\mathbf{Z}_s$, which is composing of resistors, inductors and capacitors.
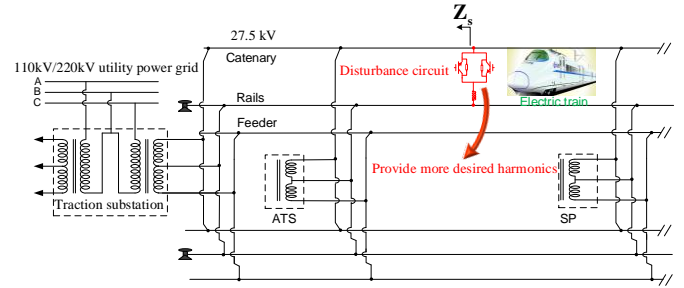


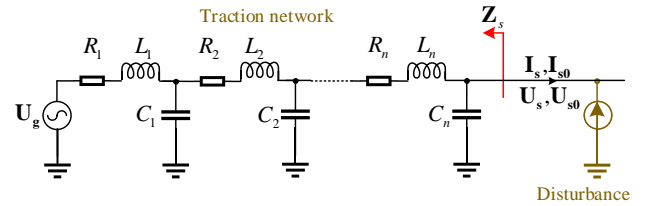Fig. 1.  Disturbance injection of AT power supply.



Fig. 2.  Equivalent measurement model of Fig. 1.

However, the measurement accuracy is always effected by the background harmonics. In order to improve the accuracy, the voltage $\mathbf{U}_{s0}$ and current $\mathbf{I}_{s0}$ of the traction network are measured firstly without imposing disturbances, which also comprises of background harmonic frequencies besides the fundamental frequency. Then, a disturbance circuit is added to produce the desired harmonics, and the responses of the voltage $\mathbf{U}_s$ and current $\mathbf{I}_s$ can be measured. It should be noted that the theoretical maintenance time of injected harmonics is dependent on the desired frequency resolution of measured impedances, which is discussed carefully in Appendix A. The Fourier transform is finally utilized to obtain frequency-domain components of measured voltages and currents, and the traction network impedance can be then calculated through (1) to avoid the effects of background harmonics [19].

$$\mathbf{Z}_s(j\omega) = \frac{\mathbf{U}_s(j\omega) - \mathbf{U}_{s0}(j\omega)}{\mathbf{I}_s(j\omega) - \mathbf{I}_{s0}(j\omega)} \qquad (1)$$

where $\mathbf{U}_s(j\omega)$ and $\mathbf{I}_s(j\omega)$ represent the voltage and current of the traction network in frequency domain after imposing dis-

turbance; $\mathbf{U}_{s0}(j\omega)$ and $\mathbf{I}_{s0}(j\omega)$ are the voltage and current in the frequency domain before imposing the disturbance.

### B. Disturbance Circuit

A disturbance circuit shown in Fig. 3 is applied to produce a current with spectral components in the desired frequency range. In detail, the primary-side of the step-down transformer is connected between the catenary and the rail, while the disturbance circuit is connected to the secondary-side. Then, the disturbance circuit, consisted of anti-parallel IGBT modules and the excitation load, produces different frequency components with different driving signals of IGBTs. Moreover, the IGBT modules are composed of series-parallel IGBT sub-components to share the voltage and current for enduring the large power. Furthermore, a smoothing capacitor is connected in parallel with the disturbance circuit for filtering out undesirable higher frequencies and operates as a snubber at the same time.
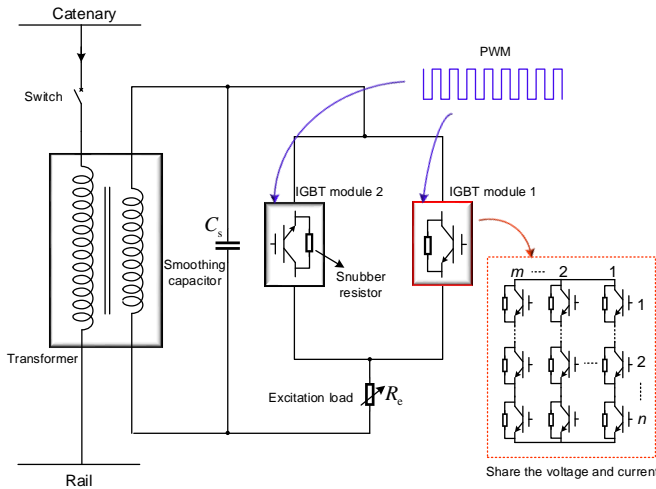


Fig. 3. Disturbance circuit to produce the desired spectral components.

The excitation load determines the power level of the harmonics excited by the disturbing circuit. Under ideal conditions, a smaller excitation load symbolizes a larger power level of the excited harmonics. In the field measurement, the value of the excitation load needs to be adjusted according to the actual system capacity for obtaining the most appropriate disturbance power. As a feasible adjustment method, at first, an excitation load with a large value is selected to bring a small harmonic level, and then reducing the excitation load to strengthen the injected power level until an accurate impedance can be measured. Moreover, in order to guarantee the safety and rational of impedance measurement, the total harmonic distortion (THD) brought by the disturbance should not exceed 5% according to "IEEE Recommended Practice and Requirements for Harmonic Control in Electric Power Systems (IEEE Std 519-2014)". Furthermore, this disturbance method can also provide spectral excitation for other AC industrial systems (e.g., renewable energy grid-connected system and AC microgrids) for measuring the corresponding network impedance. In particular, for three-phase AC systems, the impedance can be measured through imposing the disturbance in each phase, respectively.

### C. Spectral Excitation with PWM Driving signal

PWM signals are utilized to control the anti-parallel IGBT modules for generating a broad spectral excitation, as shown in Fig. 3. Moreover, all IGBTs are driven by the same control signal that can greatly simplify the control process. The time between the "ON" and "OFF" states of the IGBTs changes periodically. Meanwhile the IGBT module 1 will disturb the positive period of the current, and the negative period is perturbed by the IGBT module 2 regularly. The PWM driving signals, resulting current and voltage waveforms are presented in Fig. 4. One can find that an OFF-state of the IGBTs makes the snubber resistor and excitation load connect to the system simultaneously, which makes the response current relatively small. Then an ON-state of the IGBTs will lead to a sudden current raise as the snubber resistor is shorted and only the excitation load works. All the PWM states make periodic gaps occur in the response current, and thus a broad spectral excitation is generated.
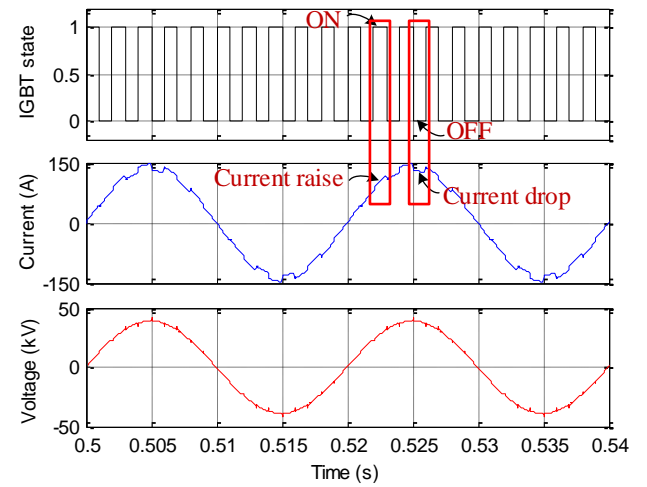


Fig. 4. PWM driving signals and the resulting current and voltage for disturbance circuit.

The PWM signal frequency is a significant parameter that determines frequency components of the excited spectrum. The injected frequencies are directly related to the frequency of the PWM driving signal.

$$f_{\text{inj}} = \left| n \times f_{\text{pwm}} \pm 50 \right| \qquad n = 1, 2, 3 \ldots \qquad (2)$$

where $f_{\text{inj}}$ is the injected frequency component; $f_{\text{pwm}}$ is the frequency of the PWM driving signal. Obviously, a lower PWM frequency will bring more abundant frequency components, which thereby gives a higher frequency resolution.

For a given case, the PWM frequency is set as 1000 Hz. It comes out that the frequencies of the excited harmonics spread at $n \times 1000 \pm 50$ Hz, $n$=1,2,3..., as presented in Fig. 5. Hence, at these frequencies, the impedances can be measured precisely. In practice, the frequency of the PWM driving signal can be set according to the actual measurement requirement of the frequency resolution.

This article has been accepted for publication in a future issue of this journal, but has not been fully edited. Content may change prior to final publication. Citation information: DOI 10.1109/TPEL.2018.2836660, IEEE Transactions on Power Electronics

> REPLACE THIS LINE WITH YOUR PAPER IDENTIFICATION NUMBER (DOUBLE-CLICK HERE TO EDIT) <          4
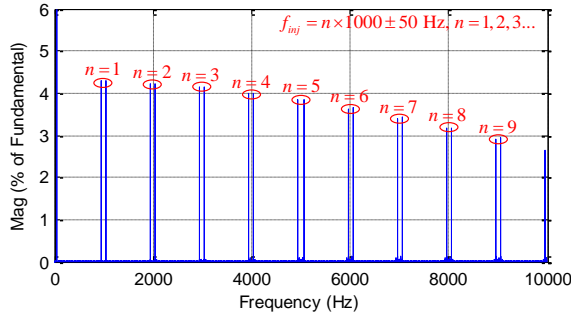
Fig. 5.  Injected harmonics when the PWM frequency is set to 1000 Hz.

Furthermore, the duty cycle of the PWM signal is also significant for excited harmonics, and it affects the distribution of the energy spectrum. The excited energy spectrum has an envelope that is periodically attenuated, and the cycle is deduced as

$$CYC_f = \begin{cases} f_{pwm} / D, & D \leq 50\% \\ f_{pwm} / (1-D), & D > 50\% \end{cases} \quad (3)$$

where $D$ is the duty cycle of the PWM driving signal; $CYC_f$ is the cycle of the envelope of excited energy spectrum.

For instance, if the duty cycle is set to 8 %, and the PWM frequency is set to 200 Hz, as a result, the excited spectrum cycle is then calculated by (3) as 200 Hz / 8% =2500 Hz, as shown in Fig. 6. In the first cycle of the spectrum distribution, the energy of the injected currents appear to be relatively maximum, and thus the impedance can be measured precisely in this frequency range. Therefore, in the field measurement, this value can be defined according to the measurement requirement of the frequency range.

Alternatively, the pseudo-random binary sequence (PRBS) can generate the similar spectrum energy distribution [20]-[22]. However, the difference is that the PRBS is generally used to disturb the closed-loop control system of the existing converter, and makes the converter output a wide spectrum excitation [20]-[22], [25]. For the electric railway system, the converters are only installed in the electric train. To ensure a smooth motion of the train, it is not allowed to add disturbances to the control system of the running train. Thus, it is not practical for the PRBS to measure the traction network impedance, and the PWM excitation combining the proposed disturbance circuit is selected here to inject the desired harmonics, not depending on the converters and associate parameters of the electric train.
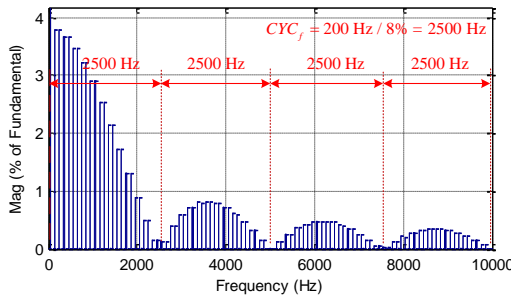


Fig. 6.  Injected harmonics when the PWM frequency is set to 200 Hz and the PWM duty cycle is set to 8 %.

### D.  Measurement Results

Based on the proposed PWM excitation principle, the desired spectrum distribution can be excited by adjusting the frequency and duty cycle of the PWM. In order to measure the traction network impedance with a 10 Hz frequency resolution, the PWM frequency just needs to be set at 10 Hz according to (2). Meanwhile, if the traction network impedance needs to be measured in the range of 10 Hz – 2000 Hz, the duty cycle of the PWM can be set to 0.5% or 99.5% to produce a large energy range just below 2000 Hz calculated by (3) to meet the requirement. The excited frequency distribution is presented in Fig. 7. It can be seen that the frequency resolution of the excited harmonics appear to be 10 Hz, and the spectrum is distributed in the broad bands with a large energy range below 2000 Hz that satisfies the requirements of the corresponding bands and frequency resolution.
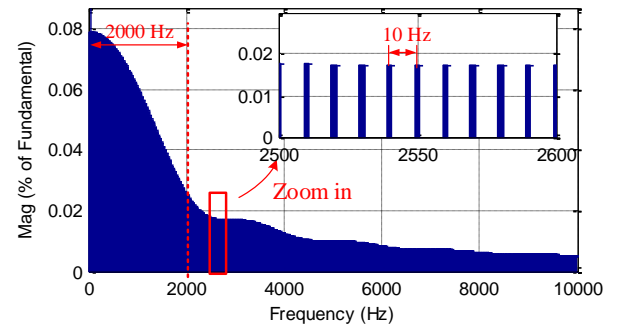


Fig. 7.  Injected harmonics when the PWM frequency is set to 10 Hz and the PWM duty cycle is set to 0.5 %.

By means of the MATLAB/SIMULINK platform, the impedance measurement model of the traction network is built to verify the correctness of the proposed method, and the simulation time step is set as $T_s = 1 \times 10^{-5}$ s . Table I lists the simulation parameters of the traction network in Fig. 2. Meanwhile, Table II gives the simulation parameters of the disturbance circuit based on the PWM driving signal. Measured results, shown in Fig. 8, illustrate that the measured impedance and theoretical value match each other well. As a result, the accuracy of the impedance measurement method is verified.

The PWM frequency of this simulation case is set as 10 Hz for obtaining the spectral excitation whose frequency resolution is 10 Hz. Fig. 9 shows the AC voltage and AC current waveforms after injecting the disturbance. As the fundamental frequency of traction power system is 50 Hz, the voltage and current waveforms will present only one disturbance spike in every 5 cycles after injecting the disturbance. Meanwhile, the voltage and current distortions caused by the disturbance are small that can be almost ignored. Thus, the method can be applied to measure the traction network impedance on line.

TABLE I
SIMULATION PARAMETERS OF THE TRACTION NETWORK

| Symbol | Parameter | Value |
|---|---|---|
| $U_g$ | Voltage source | $U_g = 27.5$ kV, $f_g = 50$ Hz |
| $R_1, R_2, R_3$ | Network-side resistors | $R_1 = 0.01$ Ω, $R_2 = 0.01$ Ω, $R_3 = 0.01$ Ω |
| $L_1, L_2, L_3$ | Network-side inductors | $L_1 = 1$ mH, $L_2 = 2$ mH, $L_3 = 3$ mH, |
| $C_1, C_2, C_3$ | Network-side capacitors | $C_1 = 0.03$ mF, $C_2 = 0.02$ mF, $C_3 = 0.01$ mF |

TABLE II
DISTURBANCE CIRCUIT PARAMETERS BASED ON PWM SIGNALS

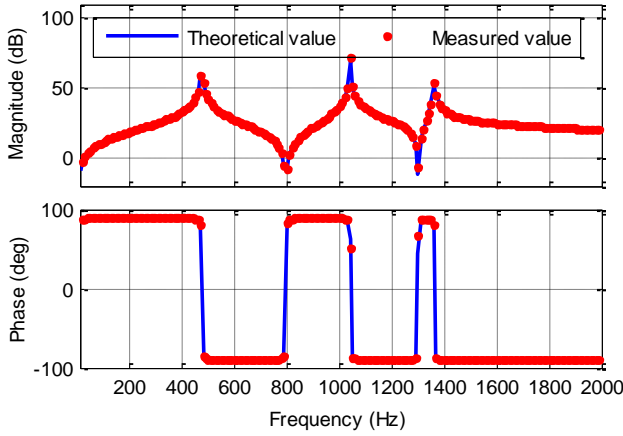| Symbol | Parameter | Value |
|--------|-----------|-------|
| $R_e$ | Excitation load | $R_e = 5\ \Omega$ |
| $f_{pwm}$ | PWM driving signal frequency | $f_{pwm} = 10$ Hz |
| $D$ | PWM driving signal duty cycle | $D = 0.5$ % |



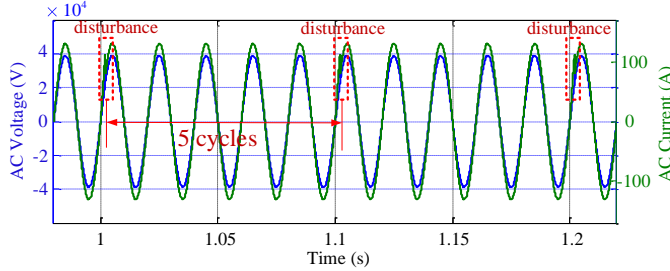Fig. 8.  The measured network impedance based on PWM driving signal.



Fig. 9.  The AC voltage and AC current at the disturbance point.

## III. IMPEDANCE MEASUREMENT OF THE 4QC OF ELECTRIC TRAIN

### A. Stationary-Frame Impedance Model

The 4QC model detailed in Fig. 10 is controlled by a dual-loop method with inductor current feedback acting as the inner loop and DC voltage feedback acting as the outer loop. The PLL can provide an angle reference for the control.
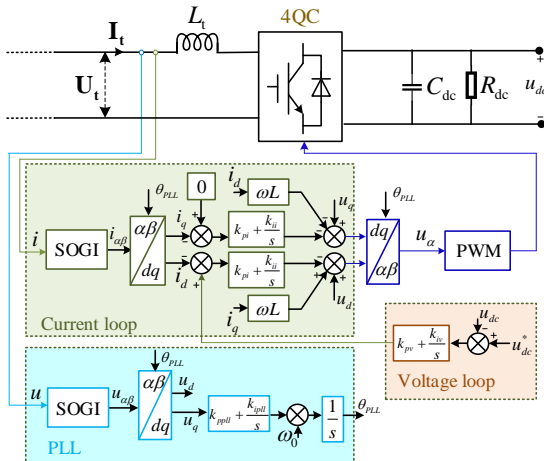


Fig. 10.  The 4QC model of electric train including control.

In order to detect a more accurate input impedance of the 4QC of electric train, the frequency coupling effect of the 4QC

should be considered during the measurement process. Otherwise, there will be a certain error in the impedance measurement results, which is discussed in Appendix B. The stationary-frame impedance matrix considering the frequency coupling effect has been proposed in [26], which is given by

$$
\begin{bmatrix} \mathbf{U}_t(j\omega) \\ e^{j2\theta}\mathbf{U}_t^*(j\omega) \end{bmatrix} = \underbrace{\begin{bmatrix} \mathbf{Z}_{t,+}(j\omega) & \mathbf{Z}_{t,-}(j\omega) \\ \mathbf{Z}_{t,-}^*(j\omega) & \mathbf{Z}_{t,+}^*(j\omega) \end{bmatrix}}_{\mathbf{Z}_{t,\pm}^m(j\omega)} \begin{bmatrix} \mathbf{I}_t(j\omega) \\ e^{j2\theta}\mathbf{I}_t^*(j\omega) \end{bmatrix} \tag{4}
$$

where $\mathbf{U}_t(j\omega)$ and $\mathbf{I}_t(j\omega)$ are the response voltage and current in frequency domain, respectively; $\mathbf{U}_t^*(j\omega)$ and $\mathbf{I}_t^*(j\omega)$ are corresponding conjugates of $\mathbf{U}_t(j\omega)$ and $\mathbf{I}_t(j\omega)$; $\mathbf{Z}_{t,\pm}^m(j\omega)$ is the impedance matrix of the 4QC in the stationary frame. It can be observed from (4) that a frequency-coupled vector at $2\omega_0-\omega$ will appear in the system for a given vector at the angular frequency $\omega$, where $\omega_0$ represents the fundamental frequency.

In order to obtain the frequency coupling impedance of the 4QC through measurement, the four components $\mathbf{Z}_{t,+}(j\omega)$, $\mathbf{Z}_{t,-}(j\omega)$, $\mathbf{Z}_{t,+}^*(j\omega)$ and $\mathbf{Z}_{t,-}^*(j\omega)$ of $\mathbf{Z}_{t,\pm}^m(j\omega)$ need to be detected. For a given voltage $\mathbf{U}_{t1}(j\omega)$, a corresponding response current $\mathbf{I}_{t1}(j\omega)$ will occur in the train-network system as well as the frequency-coupled components $e^{j2\theta}\mathbf{U}_{t1}^*(j\omega)$ and $e^{j2\theta}\mathbf{I}_{t1}^*(j\omega)$. Thus, the frequency coupling relation is then expressed by

$$
\begin{bmatrix} \mathbf{U}_{t1}(j\omega) \\ e^{j2\theta}\mathbf{U}_{t1}^*(j\omega) \end{bmatrix} = \underbrace{\begin{bmatrix} \mathbf{Z}_{t,+}(j\omega) & \mathbf{Z}_{t,-}(j\omega) \\ \mathbf{Z}_{t,-}^*(j\omega) & \mathbf{Z}_{t,+}^*(j\omega) \end{bmatrix}}_{\mathbf{Z}_{t,\pm}^m(j\omega)} \begin{bmatrix} \mathbf{I}_{t1}(j\omega) \\ e^{j2\theta}\mathbf{I}_{t1}^*(j\omega) \end{bmatrix} \tag{5}
$$

Meanwhile, for another given voltage $\mathbf{U}_{t2}(j\omega)$, it is worth noting that $\mathbf{U}_{t2}(j\omega)$ and $\mathbf{U}_{t1}(j\omega)$ are linearly independent and also at the same frequency. The frequency coupling relation can also be then expressed as

$$
\begin{bmatrix} \mathbf{U}_{t2}(j\omega) \\ e^{j2\theta}\mathbf{U}_{t2}^*(j\omega) \end{bmatrix} = \underbrace{\begin{bmatrix} \mathbf{Z}_{t,+}(j\omega) & \mathbf{Z}_{t,-}(j\omega) \\ \mathbf{Z}_{t,-}^*(j\omega) & \mathbf{Z}_{t,+}^*(j\omega) \end{bmatrix}}_{\mathbf{Z}_{t,\pm}^m(j\omega)} \begin{bmatrix} \mathbf{I}_{t2}(j\omega) \\ e^{j2\theta}\mathbf{I}_{t2}^*(j\omega) \end{bmatrix} \tag{6}
$$

Equs. (5) and (6) can be then grouped as

$$
\begin{bmatrix} \mathbf{U}_{t1}(j\omega) & \mathbf{U}_{t2}(j\omega) \\ e^{j2\theta}\mathbf{U}_{t1}^*(j\omega) & e^{j2\theta}\mathbf{U}_{t2}^*(j\omega) \end{bmatrix} = \underbrace{\begin{bmatrix} \mathbf{Z}_{t,+}(j\omega) & \mathbf{Z}_{t,-}(j\omega) \\ \mathbf{Z}_{t,-}^*(j\omega) & \mathbf{Z}_{t,+}^*(j\omega) \end{bmatrix}}_{\mathbf{Z}_{t,\pm}^m(j\omega)} \begin{bmatrix} \mathbf{I}_{t1}(j\omega) & \mathbf{I}_{t2}(j\omega) \\ e^{j2\theta}\mathbf{I}_{t1}^*(j\omega) & e^{j2\theta}\mathbf{I}_{t2}^*(j\omega) \end{bmatrix} \tag{7}
$$

As a result, the impedance matrix $\mathbf{Z}_{t,\pm}^m(j\omega)$ at the frequency $\omega$ can be then solved by

$$
\underbrace{\begin{bmatrix} \mathbf{Z}_{t,+}(j\omega) & \mathbf{Z}_{t,-}(j\omega) \\ \mathbf{Z}_{t,-}^*(j\omega) & \mathbf{Z}_{t,+}^*(j\omega) \end{bmatrix}}_{\mathbf{Z}_{t,\pm}^m(j\omega)} = \begin{bmatrix} \mathbf{U}_{t1}(j\omega) & \mathbf{U}_{t2}(j\omega) \\ e^{j2\theta}\mathbf{U}_{t1}^*(j\omega) & e^{j2\theta}\mathbf{U}_{t2}^*(j\omega) \end{bmatrix} \begin{bmatrix} \mathbf{I}_{t1}(j\omega) & \mathbf{I}_{t2}(j\omega) \\ e^{j2\theta}\mathbf{I}_{t1}^*(j\omega) & e^{j2\theta}\mathbf{I}_{t2}^*(j\omega) \end{bmatrix}^{-1} \tag{8}
$$

In order to measure the impedance of the 4QC at desired frequencies, the injected frequency $\omega$ is swept in the desired frequency range, and then the impedance matrix $\mathbf{Z}_{t,\pm}^m(j\omega)$ in the corresponding frequency range can be detected.

### B. Measurement Method

In order to measure the input impedance matrix of the 4QC presented in (8) at desired frequencies, a voltage disturbance or

current disturbance need to be injected into the electric train, as shown in Fig. 11. In the field measurement, it is unnecessary to inject the two types of disturbances simultaneously, and only one of them is needed. Moreover, the voltage disturbance is injected into the system in series, while the current disturbance is paralleled into the system.
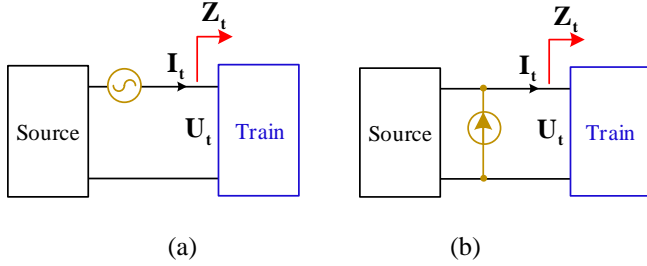


Fig. 11. Disturbance injection for impedance measurement of the 4QC. (a) Voltage disturbance. (b) Current disturbance.

Seen from (8), the two components $\mathbf{Z}_{t,+}(j\omega)$ and $\mathbf{Z}_{t,-}(j\omega)$ of $\mathbf{Z}_{t,\pm}^{m}(j\omega)$ need to be detected since the other two components $\mathbf{Z}_{t,+}^{*}(j\omega)$ and $\mathbf{Z}_{t,-}^{*}(j\omega)$ of $\mathbf{Z}_{t,\pm}^{m}(j\omega)$ can be calculated by using conjugation operation. $\mathbf{Z}_{t,+}(j\omega)$ and $\mathbf{Z}_{t,-}(j\omega)$ can be then expressed as

$$\begin{bmatrix} \mathbf{Z}_{t,+}(j\omega) \\ \mathbf{Z}_{t,-}(j\omega) \end{bmatrix} = \begin{bmatrix} \mathbf{I}_{t1}(j\omega) & e^{j2\theta}\mathbf{I}_{t1}^{*}(j\omega) \\ \mathbf{I}_{t2}(j\omega) & e^{j2\theta}\mathbf{I}_{t2}^{*}(j\omega) \end{bmatrix}^{-1} \begin{bmatrix} \mathbf{U}_{t1}(j\omega) \\ \mathbf{U}_{t2}(j\omega) \end{bmatrix} \quad (9)$$

Taking voltage disturbance injection as an example, Fig. 12 gives a detailed flowchart for measuring the 4QC impedance at desired frequencies. It involves determining the desired frequency range of impedance measurement firstly, and then two voltage vectors, which are linearly independent as well as at the same frequency ω, are injected to the system respectively for capturing the two groups of data of voltages and currents that are linearly independent. Afterwards, fast Fourier transformer (FFT) is used to analyze the captured data for extracting the voltages and currents at corresponding frequencies including the frequency-coupled components. Finally, the two components $\mathbf{Z}_{t,+}(j\omega)$ and $\mathbf{Z}_{t,-}(j\omega)$ of the impedance matrix $\mathbf{Z}_{t,\pm}^{m}(j\omega)$ can be solved by (9), and the other two components $\mathbf{Z}_{t,+}^{*}(j\omega)$ and $\mathbf{Z}_{t,-}^{*}(j\omega)$ of $\mathbf{Z}_{t,\pm}^{m}(j\omega)$ can be calculated by conjugation operation for obtaining a complete impedance matrix. The measurement process is repeated by sweeping the injected frequency ω until the 4QC impedances at all the desired frequencies are measured.
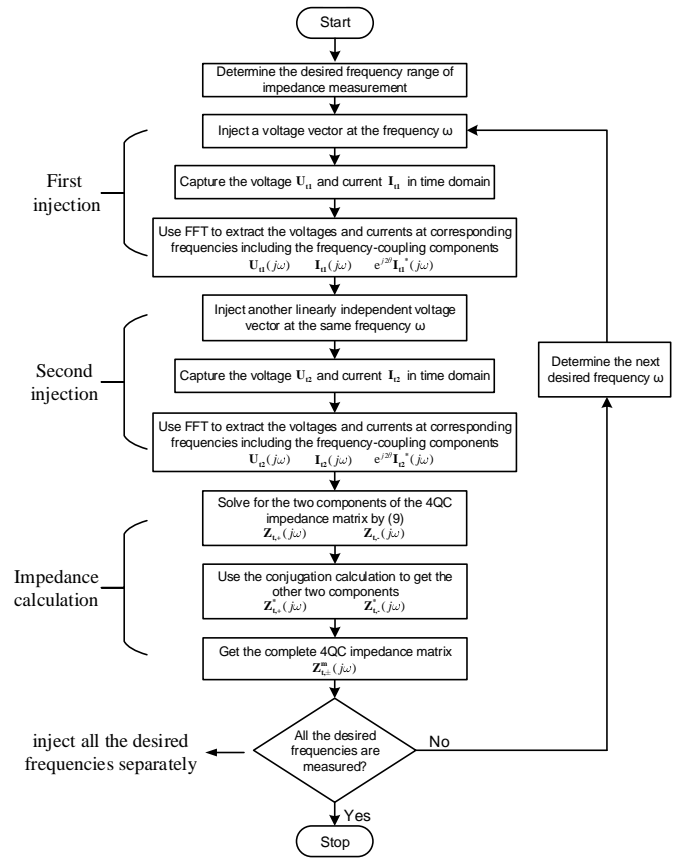


Fig. 12. The detailed flowchart for measuring the 4QC impedance.

The voltage vector is defined in the stationary frame based on values of the specific length, initial phase angle and the angular frequency. For example, $u = A\cos(\omega t + \varphi)$ can be expressed with vector by

$$u = A\cos(\omega t + \varphi) \xleftarrow{\ \omega\ } \dot{U} = A\angle\varphi \quad (10)$$

where A is the length of the vector; $\varphi$ is the initial phase angle. In order to make the description more clear, the voltage vector is shown in Fig. 13.
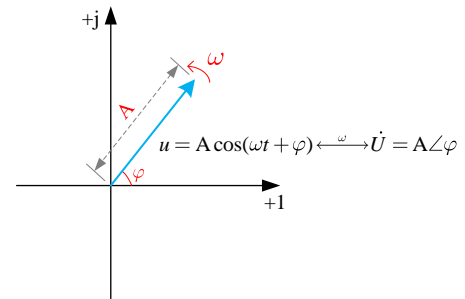


Fig. 13. The voltage vector in the stationary frame.

The two linearly independent vectors at the same frequency can be obtained by changing the initial phase of the injected vectors. For example, the two linearly independent voltage vectors at the same frequency ω can be presented by

$$\begin{cases} u_1 = A_1\cos(\omega t + \varphi_1) \\ u_2 = A_2\cos(\omega t + \varphi_2) \end{cases} \quad |\varphi_1 - \varphi_2| \neq n\times180° \quad n = 0,1,... \quad (11)$$

For clearly describing the two linearly independent vectors at the same frequency ω, the two vectors are shown in Fig. 14. $u_1$ and $u_2$ are linearly independent when these two voltage vectors are not on a line.
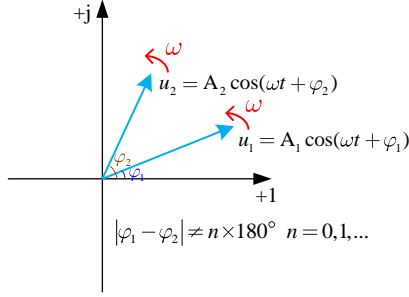


Fig. 14. Linearly independent voltage vectors at the same frequency.

### C. Simulation Results

The above proposed impedance measurement method is adopted to detect the impedance of the 4QC of electric train at the desired frequencies. This measurement will focus on the low frequency band as the reported instability of the real railway system almost happens at the low frequencies. For instance, the injected frequency is swept from 1 Hz to 150 Hz, then, the 4QC impedance can be detected at each sweeping frequency. Moreover, the train-network interaction can be analyzed by plotting the frequency responses for the eigenvalues of the 4QC impedance matrix against the traction network impedance [26] since the eigenvalues characterize some intrinsic properties of the 4QC. For this reason, the eigenvalue curves is used to describe the impedance measurement results. Simulation parameters of the train are listed in Table III.

Fig. 15 shows the eigenvalue curves of the 4QC impedance matrix determined from the simulation. As can be seen, the curves appears to be smooth, and each frequency in the range of 1 Hz − 150 Hz can be measured. Moreover, the stability of the train-network system in time domain will be discussed in next section to verify the accuracy of the impedance measurement method.

TABLE III
SIMULATION PARAMETERS OF THE TRAIN IN FIG. 10

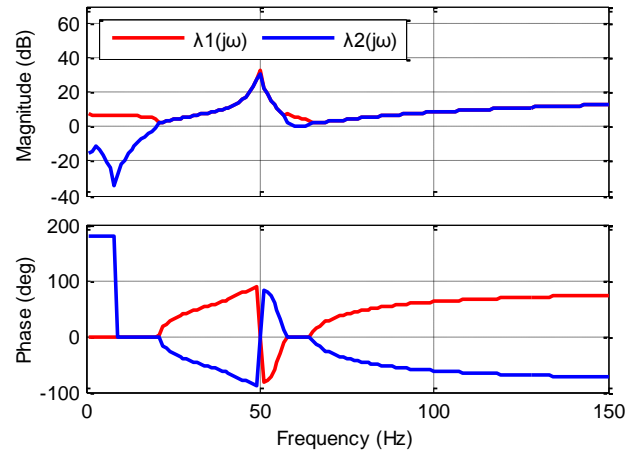| Symbol | Parameter | Value |
|---|---|---|
| $U_t$ | The input voltage of 4QC | $U_t = 1770$ V |
| $L_t$ | The 4QC inductor | $L_t = 5$ mH |
| $C_{dc}$ | Regulated capacitor | $C_{dc} = 9$ mF |
| $R_{dc}$ | DC load | $R_{dc} = 50$ Ω |
| $u_{dc}^*$ | DC voltage reference | $u_{dc}^* = 3000$ V |
| $f_s$ | Switching frequency | $f_s = 1250$ Hz |
| $K_{pi}, K_{ii}$ | PI parameters of current loop | $K_{pi} = 2, K_{ii} = 2$ |
| $K_{pv}, K_{iv}$ | PI parameters of voltage loop | $K_{pv} = 0.5, K_{iv} = 2$ |



Fig. 15. The eigenvalue curves of the measured 4QC impedance matrix

## IV. STABILITY ANALYSIS BASED ON MEASURED IMPEDANCES

### A. The Criterion for Stability

There are available methods for stability analysis in the different applications [26]-[30] wherein the impedance-based stability that can be determined by using the generalized Nyquist stability criterion is widely used [26]-[29]. The impedance ratio matrix can be defined as

$$\mathbf{L^m}(j\omega) = \mathbf{Z_s^m}(j\omega)\mathbf{Y_{t,\pm}^m}(j\omega) \tag{12}$$

where $\mathbf{Z_s^m}(j\omega)$ is the traction network impedance matrix; $\mathbf{Y_{t,\pm}^m}(j\omega)$ is the admittance matrix of the 4QC, i.e., $\mathbf{Y_{t,\pm}^m}(j\omega) = \mathbf{Z_{t,\pm}^m}(j\omega)^{-1}$. Then, the stability of the train-network system can be predicted by studying the eigenvalues of the impedance ratio matrix, which can be expressed as

$$\det[\lambda\mathbf{E} - \mathbf{Z_s^m}(j\omega)\mathbf{Y_{t,\pm}^m}(j\omega)] = 0 \tag{13}$$

where $\mathbf{E}$ is the identity matrix. The traction network impedance matrix $\mathbf{Z_s^m}(j\omega)$ appears as a diagonal matrix since the traction network is balanced, which can be derived by (14) in the stationary frame.

$$\mathbf{Z_s^m}(j\omega) = \begin{bmatrix} \mathbf{Z_s}(j\omega) & 0 \\ 0 & \mathbf{Z_s^*}(j\omega) \end{bmatrix} \tag{14}$$

Furthermore, the expression (13) can be approximated as (15) for the diagonal traction network impedance matrix [26].

$$\det[\lambda\mathbf{E} - \mathbf{Z_s^m}(j\omega)\mathbf{Y_{t,\pm}^m}(j\omega)] \approx \mathbf{Z_s}(j\omega) \cdot \det[\lambda\mathbf{E} - \mathbf{Y_{t,\pm}^m}(j\omega)] \tag{15}$$

Observed from (15), the stability can be then identified by studying the eigenvalue curves of the measured impedance matrix of the 4QC against the traction network impedance. Furthermore, as shown in (16), the phase difference at their magnitude intersection determines the phase margin [31]-[33].

$$PM = 180° - \left|\angle\mathbf{Z_s}(jw) - \angle\lambda_t(jw)\right| \tag{16}$$

where $PM$ is the phase margin; $\angle\mathbf{Z_s}(j\omega)$ and $\angle\lambda_t(j\omega)$ represent the phases of the traction network impedance and the eigenvalues of the 4QC impedance matrix, respectively. A phase difference that is far less than 180° indicates a stable system with a sufficient phase margin. Besides, a phase difference that

is close to 180 ° illustrates that the system is marginally stable with some resonant or unexpected harmonic components occurring. However, a phase difference that is out of 180 ° illustrates that the system is unstable with a negative phase margin.

### B. Oscillatory Frequency Identification

The above analysis illustrates that a phase difference close to 180 ° may make some resonant or unexpected harmonic components occur in the system. However, an unexpected inter-harmonic around 50 Hz will oscillate the system. In order to identify this oscillatory frequency, the generated inter-harmonic that overlays to the original fundamental can be expressed as

$$\text{SW} = A \cos \omega_0 t + B \cos \omega_h t \quad (17)$$

where SW is the superimposed waveform in time domain; A and B are the amplitudes of the fundamental and the generated inter-harmonic, respectively; $\omega_0$ (i.e., $\omega_0 = 2\pi f_0$) and $\omega_h$ (i.e., $\omega_h = 2\pi f_h$) are the corresponding angular frequencies, respectively. Therefore, (17) can be rewritten as

$$\text{SW} = \sqrt{\alpha^2 + \beta^2} \cdot \left[ \sin \ y - \omega_0 t \ \right] \quad (18)$$

where:

$$\begin{cases} \alpha = A + B \cos\left[ \ \omega_h - \omega_0 \ t \right] \\ \beta = B \sin\left[ \ \omega_h - \omega_0 \ t \right] \\ y = \arcsin \ \alpha \ / \ \sqrt{\alpha^2 + \beta^2} \end{cases} \quad (19)$$

Thus, the amplitude of the superimposed waveform can be then calculated as

$$\begin{aligned} \text{SW}_A &= \sqrt{\alpha^2 + \beta^2} \\ &= \sqrt{A^2 + B^2 + 2AB \cos\left[ \ \omega_h - \omega_0 \ t \right]} \end{aligned} \quad (20)$$

As can be seen from (20), the angular frequency of $\text{SW}_A$ can be obtained as

$$\omega_{\text{SW}_A} = \left| \omega_h - \omega_0 \right| \quad (21)$$

Furthermore, the amplitude oscillatory frequency of the superimposed waveform caused by the generated inter-harmonic around 50 Hz can be calculated as

$$f_{\text{osc}} = \left| f_h - f_0 \right| = \left| f_h - 50 \right| \ \text{Hz} \quad (22)$$

where $f_{\text{osc}}$ is the oscillatory frequency.

### C. Verification for the Method

In order to verify the accuracy of the measured train-network impedances and the validity of the stability analysis, a train-network simulation system is given in Fig. 16. The traction network parameters are converted to the input side of the 4QC. Initially, the train-network system remains stable as it operates with the parameters given in Table IV.
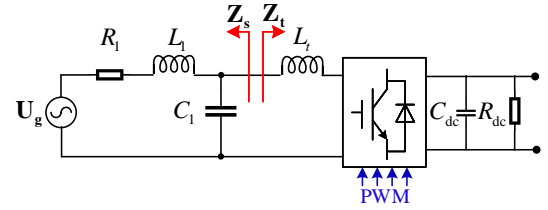


Fig. 16. Train-network simulation system.

TABLE IV
SIMULATION PARAMETERS OF THE TRAIN-NETWORK SYSTEM

| Symbol | Parameter | Value |
|---|---|---|
| $\mathbf{U_g}$ | Voltage source | $U_g = 1770$ V, $f_g = 50$ Hz |
| $R_1$ | Network-side resistor | $R_1 = 0.129$ Ω |
| $L_1$ | Network-side inductor | $L_1 = 8$ mH |
| $C_1$ | Network-side capacitor | $C_1 = 20$ μF |
| $L_t$ | The 4QC inductor | $L_t = 5$ mH |
| $C_{dc}$ | Regulated capacitor | $C_{dc} = 9$ mF |
| $R_{dc}$ | DC load | $R_{dc} = 50$ Ω |
| $u_{dc}$ | DC-link voltage | $u_{dc} = 3000$ V |
| $f_s$ | Switching frequency | $f_s = 1250$ Hz |
| $K_{pi}, K_{ii}$ | PI parameters of current loop | $K_{pi} = 2, K_{ii} = 2$ |
| $K_{pv}, K_{iv}$ | PI parameters of voltage loop | $K_{pv} = 0.5, K_{iv} = 2$ |

The equivalent inductance of the traction network that is mainly composed of three parts: the equivalent inductances of the utility power grid, traction transformer and catenary network is presented in Appendix C. However, the train running at different positions of the catenary symbolizes the different equivalent length of the supplied catenary network. Obviously, a longer supplied catenary will bring a larger equivalent inductance. For instance, when the network equivalent inductance $L_1$ is increased from the original 8 mH to 10 mH owing to the increase of the equivalent catenary length, the traction network will be weakened. Fig. 17(a) depicts the measured traction network impedance and the eigenvalues of the measured impedance matrix of the 4QC. One can observe that the phase difference at the magnitude intersection frequency 55 Hz is 168 °. Thus, the phase margin that is only 12 ° illustrates that the resonant or unexpected inter-harmonic component nearby 55 Hz may be excited in the train-network system. Moreover, it will bring a frequency-coupled component at 45 Hz to the system according to (4), as shown in Fig. 18(a), which illustrates that an oscillation with a frequency of 5 Hz calculated by (22) will occur in the train-network system. Fig. 19(a) shows the AC voltage, AC current and DC voltage waveforms, and it can be found that the oscillatory frequency actually appears to be 5 Hz in time domain, keeping consistent with the impedance-based stability analysis results.

For another case, the network equivalent inductor $L_1$ that is increased to 12.5 mH makes the magnitude intersection frequency vary accordingly. As a measured result, Fig. 17(b) shows the traction network impedance and associated eigenvalues of the measured 4QC impedance matrix. The magnitude intersection frequency is 54 Hz and the phase difference is 174 ° that brings a weak phase margin of only 6 ° accordingly. It illustrates that the resonant or unexpected inter-harmonic component nearby 54 Hz occurs in this system that will bring a frequency-coupled component at 46 Hz according to (4), shown in Fig. 18(b). Thus, this system will oscillate with a 4 Hz frequency calculated by (22), which keeps consistent with the oscillation in time domain as shown in Fig. 19(b). Therefore,

the accuracy of the measured train-network impedances is further validated by the stability analysis results.

Before the train is put into operation, the train-network impedances can be measured to forecast whether the instability or oscillation will occur, and determine whether the parameters of the electric train are reasonable in order to ensure a safe and stable operation of the high-speed railway.
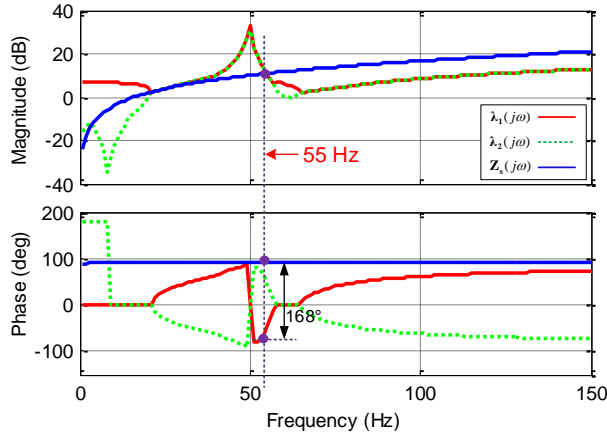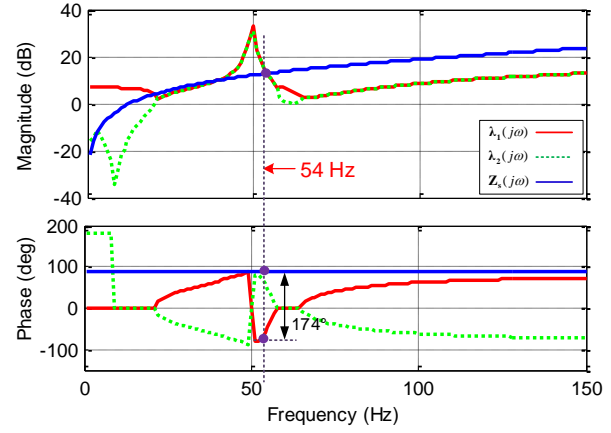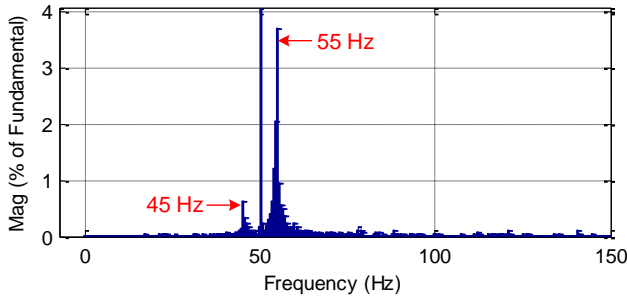


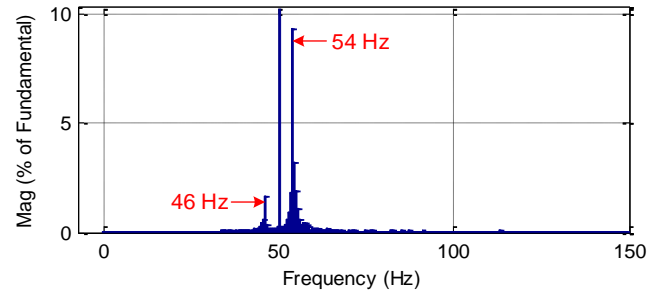Fig. 17. Frequency responses for the eigenvalues of the 4QC impedance matrix and the traction network impedance after increasing the network-side inductor. (a) Increasing L1 to 10 mH. (b) Increasing L1 to 12.5 mH.



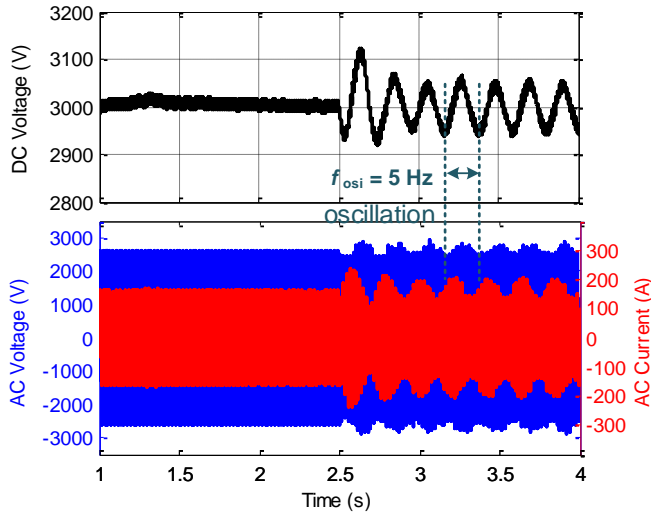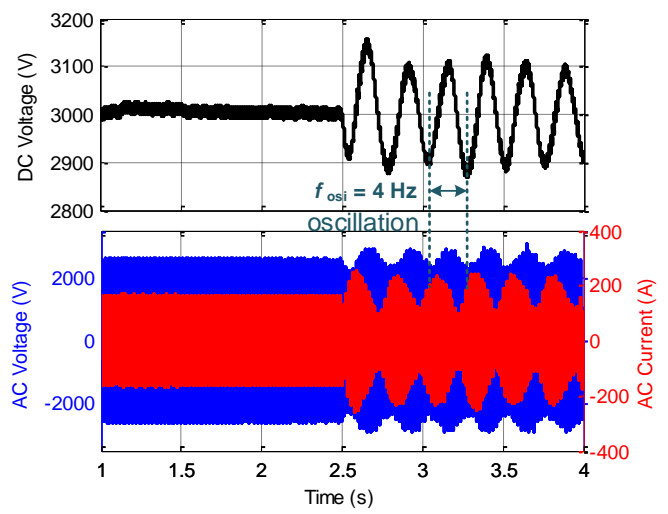Fig. 18. AC voltage spectrum after increasing the network-side inductor. (a) Increasing L1 to 10 mH. (b) Increasing L1 to 12.5 mH.



Fig. 19. AC voltage, AC current and DC voltage waveforms. (a) Increasing L1 to 10 mH. (b) Increasing (L1 to 12.5 mH.

## V. Experimental Validation

### A. Experimental System

A train-network experimental system including the disturbance circuit, shown in Fig. 20 and Fig. 21, is conducted to validate the effectiveness of the impedance measurement method for the stability analysis, and the electric parameters of the experimental system are listed in Table V. The IGBTs of the disturbance circuit and the experimental 4QC of electric train are controlled by a DSP 28335 control system. Besides, the electrical signals acquisition device is used to measure the data of voltage and current, and then do data processing by MATLAB to calculate the impedances of the electric train and traction network.

In the measurement process, the traction network impedance is first measured via the proposed method in Section II, and then measure the frequency coupling impedance of the 4QC. After that, the impedance-based stability analysis can be implemented to prejudge the stability state before the train accesses to the traction network. Finally, the actual stability performance of the train-network experimental system can be observed to verify the accuracy of the proposed impedance measurement and stability analysis.
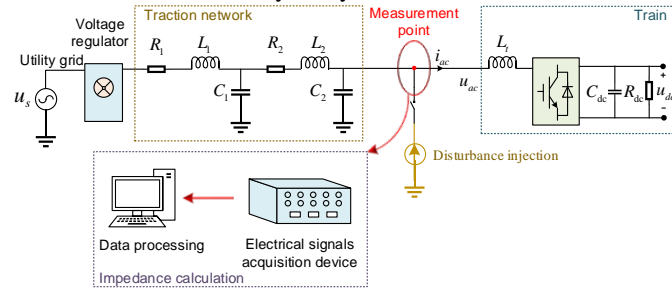


Fig. 20. Diagram of impedance measurement.

TABLE V
TRAIN-NETWORK EXPERIMENTAL SYSTEM PARAMETERS

| Symbol | Parameter | Value |
|---|---|---|
| $u_s$ | Utility power grid voltage | $u_s$ = 220 V |
| $R_1, R_2$ | Network-side resistors | $R_1$ = 0.7 Ω, $R_2$ = 0.54 Ω |
| $L_1, L_2$ | Network-side inductors | $L_1$ = 16.1 mH, $L_2$ = 12.4 mH |
| $C_1, C_2$ | Network-side capacitors | $C_1$ = 0.94 μF, $C_2$ = 0.44 μF |
| $R_{dc}$ | DC-side load | $R_{dc}$ = 200 Ω |
| $L_t$ | The input inductor of 4QC | $L_t$ = 14.1 mH |
| $C_{dc}$ | DC capacitor | $C_{dc}$ = 0.44 μF |
| $u_{dc}$ | DC-link voltage | $u_{dc}$ = 42 V |
| $f_s$ | Switching frequency | $f_s$ = 1250 Hz |
| $K_{pi}, K_{ii}$ | PI parameters of current loop | $K_{pi}$ = 4, $K_{ii}$ = 0.15 |
| $K_{pv}, K_{iv}$ | PI parameters of voltage loop | $K_{pv}$ = 0.1, $K_{iv}$ = 0.002 |
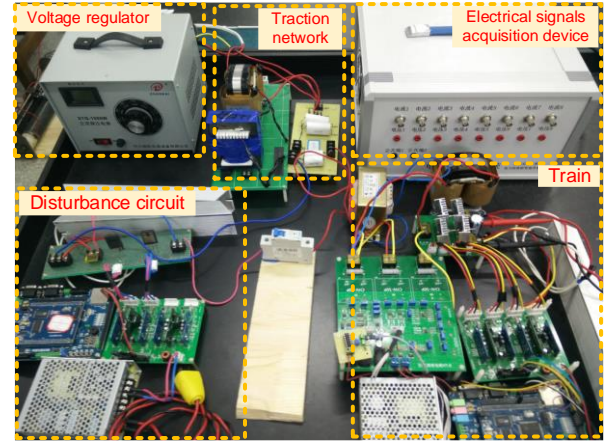


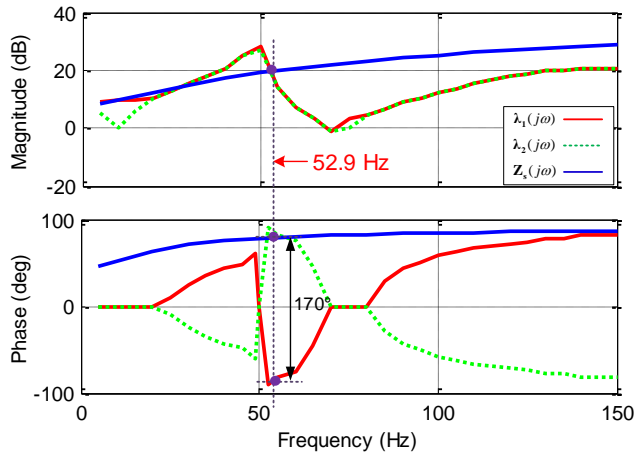Fig. 21. Experimental device of impedance measurement.

### B. Experimental Results

Fig. 22(a) shows the measured traction network impedance and the associated eigenvalues of the measured 4QC impedance matrix based on the experimental system. It can be seen that the phase difference at the magnitude intersection frequency 52.9 Hz is 170 ° that symbolizes a phase margin of only 10 °, and may cause the inter-harmonic 52.9 Hz component in the system. Thus, an amplitude oscillation of 2.9 Hz, calculated by (22), occurs in the experimental system. The actual oscillatory frequency in time domain is 3 Hz as shown in Fig. 22(b), and the error can be acceptable.
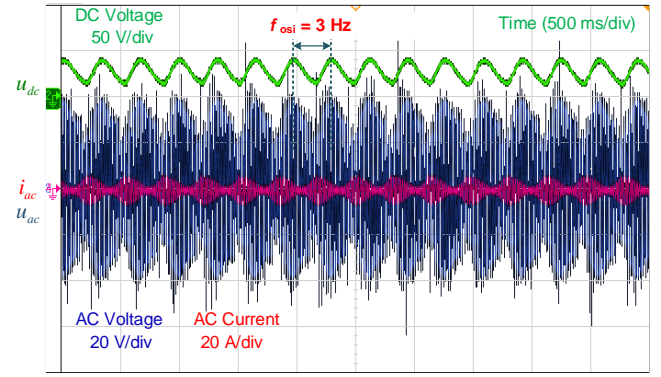
Then, the network equivalent inductor $L_1$ is increased to 20.4 mH, and $L_2$ is increased to 17.4 mH that makes the magnitude intersection frequency vary accordingly. As a measured result, the traction network impedance and the eigenvalues of the measured 4QC impedance matrix being presented in Fig. 23(a) shows that the magnitude intersection frequency is 52 Hz, and the phase difference is 172 ° (i.e., phase margin is 8 °). Therefore, the resonant or unexpected inter-harmonic component nearby 52 Hz may occur in the system, which oscillate this system with a frequency of 2 Hz calculated by (22). The actual oscillatory frequency in time domain is 2.1 Hz as shown in Fig. 23(b).

Finally, reducing the network-side inductors $L_1$ and $L_2$ to 1 mH and 2 mH respectively, the traction network impedance magnitude curve will drop as shown in Fig. 24(a). One can find that the phase differences of all the magnitude curves intersections are far smaller than 180 ° that indicates the system is definitely stable and will not produce the unexpected harmonic as shown in Fig. 24(b).

The measured impedances curves of the traction network and the eigenvalues of the 4QC impedance matrix appear to be smooth, and have the same behaviors as simulation values. Besides, in the acceptable range of deviation, the oscillatory frequency calculated by the magnitude intersection frequency can match the actual oscillatory frequency in time domain, which verifies the correctness of the measured train-network impedances and the effectiveness of the measurement method.

This article has been accepted for publication in a future issue of this journal, but has not been fully edited. Content may change prior to final publication. Citation information: DOI 10.1109/TPEL.2018.2836660, IEEE Transactions on Power Electronics

> REPLACE THIS LINE WITH YOUR PAPER IDENTIFICATION NUMBER (DOUBLE-CLICK HERE TO EDIT) <     11



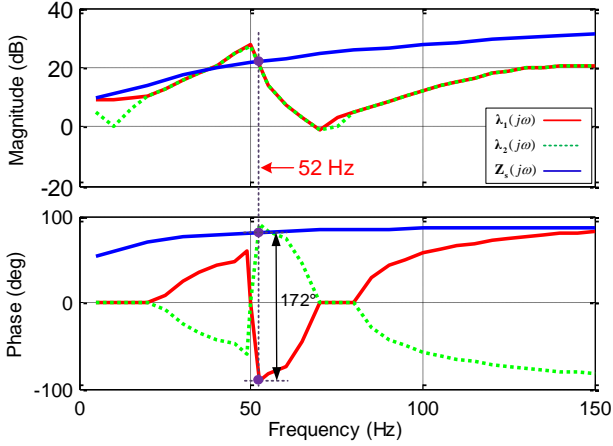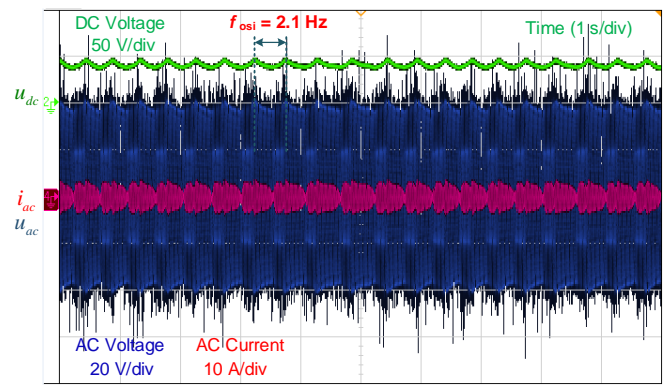(a)                                    (b)

Fig. 22.  Train-network impedance measurement results and stability analysis. (a) The matching curves of train-network impedances. (b) Measured AC voltage, AC current and DC voltage.



(a)                                    (b)

Fig. 23.  Train-network impedance measurement results and stability analysis after increasing the network-side inductor. (a) The matching curves of train-network impedances. (b) Measured AC voltage, AC current and DC voltage.
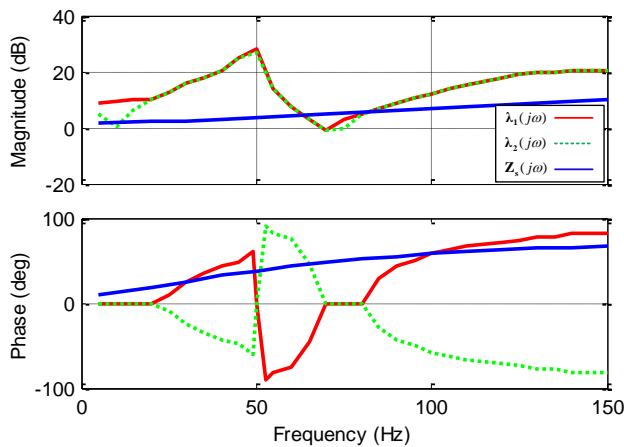


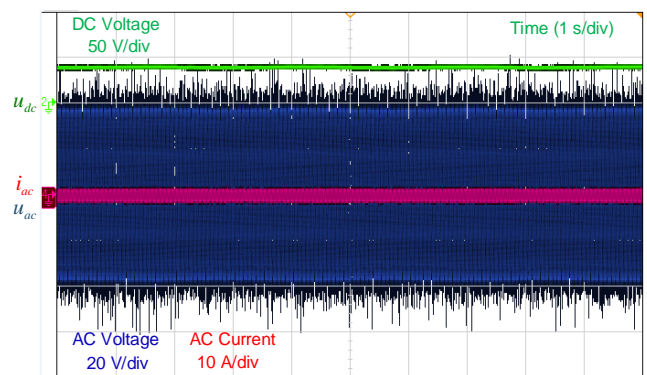(a)                                    (b)

Fig. 24.  Train-network impedance measurement results and stability analysis after reducing the network-side inductor. (a) The matching curves of train-network impedances. (b) Measured AC voltage, AC current and DC voltage.

## VI. CONCLUSION

This paper presents a train-network impedance measurement method, and uses the matching relation of the measured train-network impedances to identify the stability issues. A desired broad spectral excitation method by means of the PWM signal has been proposed to detect the accurate traction network impedance. Then, considering the frequency coupling effect, an effective impedance measurement method of the 4QC of electric train has further been introduced. Moreover, based on the magnitude intersection frequency of the measured traction network impedance and the eigenvalues of the measured 4QC impedance matrix, the resonant or unexpected harmonic component can be identified as well as the oscillatory frequency. The proposed method has been verified by simulations and experiments. Before the train is put into operation, the impedance measurement and stability analysis can be used to forecast the stability of the high-speed railways to ensure a safe and stable operation of this system.

## APPENDIX A

This Appendix presents the theoretical maintenance time of injected harmonics. FFT transforms the captured signals in time domain into the frequency domain, and the frequency resolution of the transformation results is given by

$$\Delta f = \frac{f_s}{N} \tag{A1}$$

where $\Delta f$ is the frequency resolution of the FFT results; $f_s$ is sampling frequency; $N$ is the number of sampling points, and can be calculated by

$$N = \frac{t}{T_s} = t \cdot f_s \tag{A2}$$

where $t$ is sampling time; $T_s$ is sampling period. Combining with (A1) can be converted as

$$\Delta f = \frac{1}{t} \tag{A3}$$

Thus, the sampling time can be presented as

$$t = \frac{1}{\Delta f} \tag{A4}$$

For example, when the desired frequency resolution is 50 Hz, the sampling time is calculated as $t = 1/50 = 0.02$ s according to (A4). Thus, the theoretical maintenance time of injected harmonics is 0.02 s as shown in Fig. A1(a). When the desired frequency resolution is 10 Hz, the sampling time is calculated as $t = 1/10 = 0.1$ s . Thus, the theoretical maintenance time is 0.1 s as shown in Fig. A1(b).
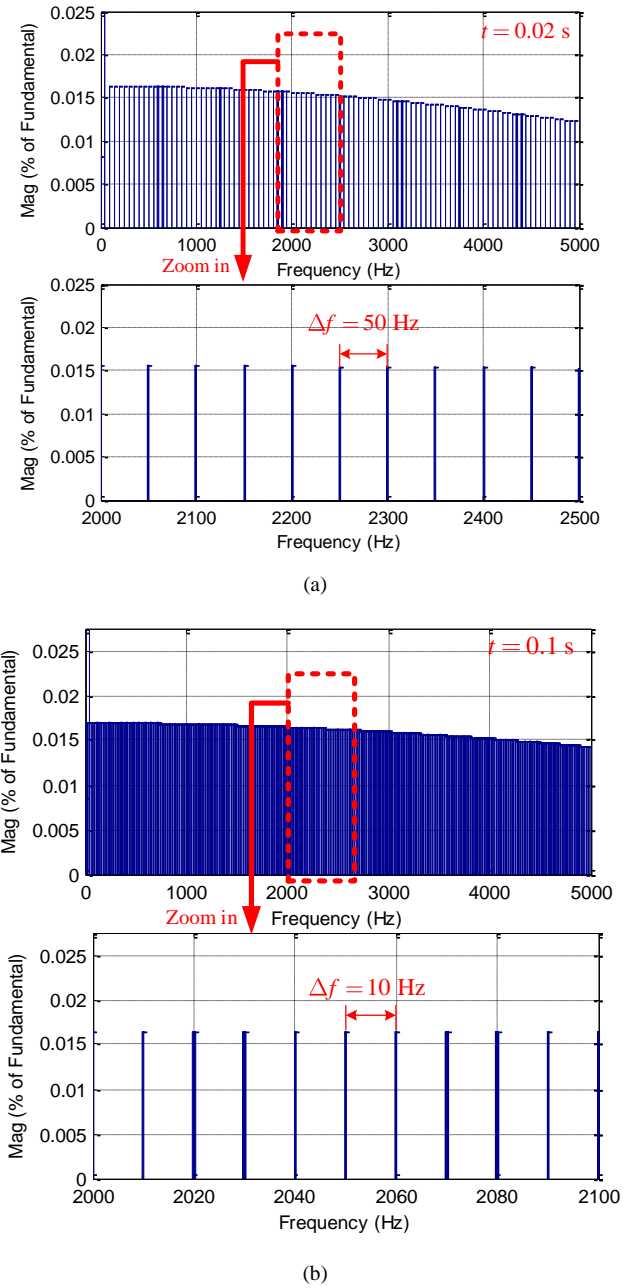


Fig. A1. The frequency resolution of the FFT results. (a) When the sampling time is 0.02 s. (b) When the sampling time is 0.1 s.

In summary, the theoretical maintenance time of injected harmonics is related to the desired frequency resolution of measured impedances. When the desired frequency resolution is higher, the sampling time should be longer that symbolized a longer maintenance time of the injected harmonics.

## APPENDIX B

This Appendix presents the impedance measurement result without considering the frequency coupling. The stationary-frame impedance matrix without considering the frequency coupling effect is given by

$$\begin{bmatrix} \mathbf{U}_t(j\omega) \\ e^{j2\theta}\mathbf{U}_t^*(j\omega) \end{bmatrix} = \underbrace{\begin{bmatrix} \mathbf{Z}_{t,+}(j\omega) & 0 \\ 0 & \mathbf{Z}_{t,+}^*(j\omega) \end{bmatrix}}_{\mathbf{Z}_{t,\pm}^m(j\omega)} \begin{bmatrix} \mathbf{I}_t(j\omega) \\ e^{j2\theta}\mathbf{I}_t^*(j\omega) \end{bmatrix} \tag{A5}$$

This article has been accepted for publication in a future issue of this journal, but has not been fully edited. Content may change prior to final publication. Citation information: DOI 10.1109/TPEL.2018.2836660, IEEE Transactions on Power Electronics

> REPLACE THIS LINE WITH YOUR PAPER IDENTIFICATION NUMBER (DOUBLE-CLICK HERE TO EDIT) <       13

where $\mathbf{U}_t(j\omega)$ and $\mathbf{I}_t(j\omega)$ are the response voltage and current in frequency domain; $e^{j2\theta}\mathbf{U}_t^*(j\omega)$ and $e^{j2\theta}\mathbf{I}_t^*(j\omega)$ are the frequency coupling components; $\mathbf{Z}_{t,\pm}^m(j\omega)$ is the 4QC impedance matrix without considering the frequency coupling effect in the stationary frame.

The traction network and 4QC parameters are set as shown in Table IV. When increasing the equivalent length of the catenary, the equivalent inductance of the traction network $L_1$ will be increased from the original 8 mH to 10 mH, and the traction network will be weakened. Fig. A2 depicts the measured traction network impedance and the eigenvalues of the measured 4QC impedance matrix. The magnitude intersection frequency is seen at 52.8 Hz, and at this frequency, the phase difference is 169 °that indicates that the phase margin is only 11 °. This weak phase margin illustrates that the resonant or unexpected inter-harmonic component nearby 52.8 Hz may occur in the system. Thus, this system will oscillate with a 2.8 Hz frequency based on the measured impedances. However, the actual oscillation frequency in time domain is 4 Hz as shown in Fig. A3. Thus, there is a certain error without considering the frequency coupling. Therefore, the frequency coupling effect should be taken into account.
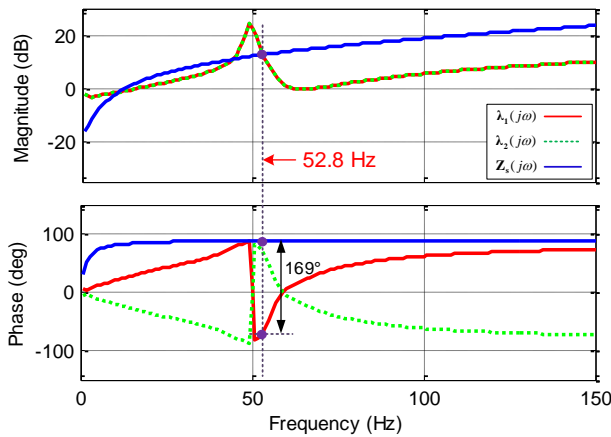


Fig. A2. The measured traction network impedance and the eigenvalues of the measured 4QC impedance matrix
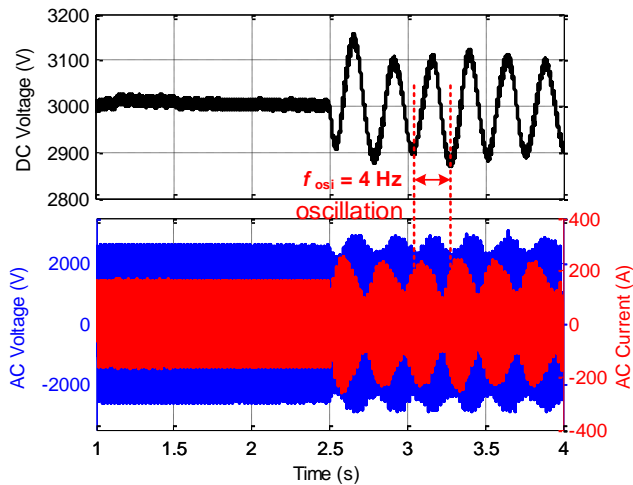


Fig. A3. The AC voltage, AC current and DC voltage waves.

## APPENDIX C

The detailed impedance calculation of the whole traction network can be found in [34], which is mainly composed of three parts. 1) Utility power grid; 2) Traction transformer; 3) Catenary network. These impedances are further used to determine the equivalent parameters of the simulation and experimental system.

The equivalent inductance of utility power grid and traction transformer keeps almost constant owing to its constant parameters. However, when the train runs to different locations of the catenary, the equivalent length of the catenary will be different. A longer catenary will bring a bigger equivalent inductance. According to the practical system parameters, the equivalent inductance and resistance of traction network can be then calculated.

## REFERENCES

[1] N. Sokal, "System oscillations from negative input resistance at power input port of switching-mode regulator, dc/dc converter, or dc/ac inverter," in *Proc. IEEE Power Electron. Spec. Conf.*, Sep. 1973, pp. 138-140.

[2] X. Wang, F. Blaabjerg, M. Liserre, Z. Chen, Y. W. Li, and J. He, "An active damper for stabilizing power-electronics-based as systems," *IEEE Trans. Power Electron.*, vol. 29, no. 7, pp. 3318-3329, Jul. 2014.

[3] X. Wang, F. Blaabjerg, and W. Wu, "Modeling and analysis of harmonic stability in ac power-electronics-based power system," *IEEE Trans. Power Electron.*, vol. 29, no. 12, pp. 6421-6432, Dec. 2014.

[4] J. H. R. Enslin and P. J. M. Heskes, "Harmonic interaction between a large number of distributed power inverters and the distribution network," *IEEE Trans. Power Electron.*, vol. 19, no. 6, pp. 1586-1593, Nov. 2004.

[5] M. Cespedes and J. Sun, "Renewable energy systems instability involving grid-parallel inverters," in *Proc. 24th Annu. Appl. Power Electron. Conf., Expo.*, Mar. 2009, pp. 1971-1977.

[6] H. Hu, H. Tao, F. Blaabjerg, X. Wang, Z. He, and S. Gao, "Train-Network Interactions and Stability Evaluation in High-Speed Railways--Part I: Phenomena and Modeling," *IEEE Trans. Power Electron.*, vol. 33, no. 6, pp. 4627-4642, Jun. 2018.

[7] H. Hu, H. Tao, X. Wang, F. Blaabjerg, Z. He, and S. Gao, "Train-Network Interactions and Stability Evaluation in High-Speed Railways--Part II: Influential Factors and Verifications," *IEEE Trans. Power Electron.*, vol. 33, no. 6, pp. 4643-4659, Jun. 2018.

[8] B. Wen, D. Boroyevich, R. Burgos, P.Mattavelli, and Z. Shen, "Analysis of D-Q small-signal impedance of grid-tied inverters," *IEEE Trans. Power Electron.*, vol. 31, no. 1, pp. 675-687, Jan. 2016.

[9] S.Vesti, T. Suntio, J. A. Oliver, R. Prieto, and J. A. Cobos, "Impedance-based stability and transient-performance assessment applying maximum peak criteria," *IEEE Trans. Power Electron.*, vol. 28, no. 5, pp. 2099-2104, May. 2013.

[10] B. Wen, D. Boroyevich, P.Mattavelli, Z. Shen, and R. Burgos, "Influence of phase-locked loop on input admittance of three-phase voltage-source converters," in *Proc. 28th Annu. Appl. Power Electron. Conf., Expo.*, Mar. 2013, pp. 897-904.

[11] Yong Li, Qianyi Liu, Sijia Hu, Fang Liu, Yijia Cao, Longfu Luo, and Christian Rehtanz, "A Virtual Impedance Comprehensive Control Strategy for the Controllably Inductive Power Filtering System," *IEEE Trans. Power Electron.*, vol. 32, no. 2, pp. 920-926, February 2017.

[12] Y. Panov and M. M. Jovanovic, "Stability and dynamic performance of current-sharing control for paralleled voltage regulator modules," *IEEE Trans. Power Electron.*, vol. 17, no. 2, pp. 172-179, Mar. 2002.

[13] Y. Tang, P. C. Loh, P. Wang, F. H. Choo, and F. Gao, "Exploring inherent damping characteristic of LCL-filters for three-phase grid-connected voltage source inverters," *IEEE Trans. Power Electron.*, vol. 27, no. 3, pp. 1433-1443, Mar. 2012.

[14] S. Cobreces, E. J. Bueno, D. Pizarro, F. J. Rodriguez, and F. Huerta, "Grid impedance monitoring system for distributed power generation electronic interfaces," *IEEE Trans. Instrum. Meas.*, vol. 58, no. 9, pp. 3112-3121, Sep. 2009.

[15] J. Yang, W. Li, T. Chen, W. Xu, and M. Wu, "Online estimation and application of power grid impedance matrices based on synchronized phasor measurements," *IET Gener., Transm. Distrib*., vol. 4, no. 9, pp. 1052-1059, Sep. 2010.

[16] M. Ciobotaru, V. Agelidis, R. Teodorescu, "Line impedance estimation using model based identification technique," in *Proc. IEEE Power Electron. Appl. Conf*., Aug. 2011, pp. 1-9.

[17] H. Gu, X. Guo, D. Wang, and W. Wu, "Real-time grid impedance estimation technique for grid-connected power converters," in *Proc. IEEE Ind Electron. Conf*., May. 2012, pp. 1621-1626.

[18] H. Jing, K. A. Corzine, and M. Belkhayat, "Small-signal impedance measurement of power-electronics-based ac power systems using line-to-line current injection," *IEEE Trans. Power Electron*., vol. 24, no. 2, pp. 445-455, Feb. 2009.

[19] M. Jordan, H. Langkowski, T. D. Thanh, and D. Schulz, "Frequency dependent grid-impedance determination with pulse-width-modulation-signals," in *Proc. 7th Int. Conf. –Workshop Compat. Power Electron*., Jun. 2011, pp. 131-136.

[20] T. Roinila, M. Vilkko, and J. Sun, "Broadband methods for online grid impedance measurement," in *Proc. IEEE Energy Convers. Congr. Expo*., *ECCE* Sep. 2013, pp. 3003-3010.

[21] T. Roinila, T. Messo and E. Santi, "MIMO-Identification Techniques for Rapid Impedance-Based Stability Assessment of Three-Phase Systems in DQ Domain," *IEEE Trans. Power Electron*, vol. 33, no. 5, pp. 4015-4022, May 2018.

[22] T. Roinila, M. Vilkko, and J. Sun, "Online grid impedance measurement using discrete-interval binary sequence injection," *IEEE Trans. Ind. Electron*., vol. 2, no. 4 pp. 985-993, Dec. 2014.

[23] Z. He, H. Hu, Y. Zhang and S. Gao, "Harmonic Resonance Assessment to Traction Power-Supply System Considering Train Model in China High-Speed Railway," *IEEE Tran. Power Del.*, vol. 29, no. 4, pp. 1735-1743, Aug. 2014.

[24] H. Hu, Y. Shao, L. Tang, J. Ma, Z. He and S. Gao. "Overview of Harmonic and Resonance in Railway Electrification Systems," *IEEE Trans. Ind. Appl.*, 2018.

[25] D. Martin, I. Nam, J. Siegers, and E. Santi, "Wide bandwidth three-phase impedance identification using existing power electronics inverter," in *Applied Power Electronics Conference and Exposition (APEC), 2013 Twenty-eighth Annual IEEE*, March 2013, pp. 334-341.

[26] X. Wang, L. Harnefors, F. Blaabjerg, "Unified impedance model of grid-connected voltage-source converters," *IEEE Trans. Power Electron*., vol. 33, no. 2, pp. 1775-1787, Feb. 2018.

[27] B. Wen, D. Boroyevich, R. Burgos, P. Mattavelli, and Z. Shen, "Small-signal stability analysis of three-phase as systems in the presence of constant power loads based on measured d-q frame impedances," *IEEE Trans. Power Electron*., vol. 30, no. 10, pp. 5952-5963, Dec. 2015.

[28] H. Tao, H. Hu, X. Wang, F. Blaabjerg, Z. He, "Impedance-Based Harmonic Instability Assessment in Multiple Electric Trains and Traction Network Interaction System," *IEEE Trans. Ind. Appl.*, 2018. To be published, DOI: 10.1109/TIA.2018.2793843.

[29] H. Hu, Y. Zhou, J. Yang, Z. He and S. Gao, "A Practical Approach to Mitigate Low-Frequency Oscillation in Railway Electrification Systems," *IEEE Trans. Power Electron.*, 2018. To be published, DOI 10.1109/TPEL.2018.2803176

[30] W. Li, L. Liang, W. Liu, X. Wu, "State of Charge Estimation of Lithium Ion Batteries Using a Discrete Time Nonlinear Observer," *IEEE Trans. Ind. Electron.*, vol. 64, no.11, pp.8557-8565, 2017.

[31] Y. Wang, X. Wang, F. Blaabjerg, "Frequency scanning-based stability analysis method for grid-connected inverter system," in *Proc. 3rd IEEE Int. Conf. Future Energy Electronics*., *ECCE-Asia* Jun. 2017, pp. 1575-1580.

[32] Y. Wang, X. Wang, F. Blaabjerg, and Z. Chen, "Harmonic resonance assessment of multiple paralleled grid-connected inverters system," in *Proc. 3rd IEEE Int. Conf. Future Energy Electronics*., *ECCE-Asia* Jun. 2017, pp. 2070-2075.

[33] Y. Song, X. Wang, F. Blaabjerg, "Impedance-based high-frequency resonance analysis of DFIG system in weak grids," *IEEE Trans. Power Electron*., vol. 32, no. 5, pp. 3536-3548, May. 2017.

[34] X. Jiang, H. Hu, Z. He, H. Tao and Q. Qian "Study on low-frequency voltage fluctuation of traction power supply system introduced by

multiple modern trains," *Electric Power Systems Research*, no. 146, pp. 246-257, 2017.